

# **The influence of elevated $\text{SiO}_2(aq)$ on intracellular silica uptake and microbial metabolism**

Rosalie Tostevin<sup>1,2\*</sup>, Joseph Snow<sup>2</sup>, Qiong Zhang<sup>2</sup>, Nicholas J. Tosca<sup>2</sup>, Rosalind E. M. Rickaby<sup>2</sup>

<sup>1</sup>Department of Geological Sciences, University of Cape Town, Rondebosch, Cape Town  
7701, South Africa.

<sup>2</sup>Department of Earth Science, University of Oxford, South Parks Road, UK, OX13AN

\*Corresponding author: Rosalie.tostevin@uct.ac.za.

**Keywords:** Archean, Proterozoic, silica, microbial metabolism, culturing

## **ABSTRACT**

Microbes are known to accumulate intracellular  $\text{SiO}_2(aq)$  up to 100s of  $\text{mmol.l}^{-1}$  from modern seawater ( $\text{SiO}_2(aq) < 100 \mu\text{mol.l}^{-1}$ ), despite having no known nutrient requirement for Si. Before the evolution of siliceous skeletons, marine silica concentrations were likely an order of magnitude higher than the modern ocean, raising the possibility that intracellular  $\text{SiO}_2(aq)$  accumulation interfered with normal cellular function in non-silicifying algae. Yet, because few culturing studies have isolated the effects of  $\text{SiO}_2(aq)$  at high concentration, the potential impact of elevated marine silica on early microbial evolution is unknown. Here, we test the influence of elevated  $\text{SiO}_2(aq)$  on eukaryotic algae, as well as a prokaryote species. Our results demonstrate that under  $\text{SiO}_2(aq)$  concentrations relevant to ancient seawater, intracellular Si accumulates to concentrations comparable to those found in siliceous algae such as diatoms. In addition, all eukaryotic algae showed a statistically significant response to the high-Si treatment, including reduced average cell sizes and/or a reduction in the maximum growth rate. In contrast, there was no consistent response to the high-Si treatment by the prokaryote species. Our results highlight the possibility that

elevated marine  $\text{SiO}_2(aq)$  may have been an environmental stressor during early eukaryotic evolution.

## 1. INTRODUCTION

The sedimentary record indicates that marine dissolved silica concentrations declined dramatically from the Precambrian (>541 million years ago, Ma) and through the Phanerozoic. For example, syndepositional and early diagenetic microcrystalline quartz (or chert) is essentially ubiquitous in peritidal sedimentary deposits spanning most of the Precambrian (Maliva et al., 2005, 1989). In addition, Archean sedimentary successions preserve petrographic evidence for primary silica precipitation and sedimentation on continental margins and in deeper basinal settings (Figure 1) (Rasmussen et al., 2015; Stefurak et al., 2015). Collectively, these observations indicate that global average  $\text{SiO}_2(aq)$  may have been poised as high as cristobalite or amorphous silica saturation, corresponding to concentrations between 0.67 and 2.2  $\text{mmol.l}^{-1}$  (Siever, 1992; Siever and Woodford, 1973). The postulated Neoproterozoic origins of siliceous sponges, and their later Cambrian radiation, may have driven a modest decrease in marine  $\text{SiO}_2$  levels, but early diagenetic chert remains a dominant component throughout much of the Palaeozoic Era (Figure 1) (Brocks et al., 2017; Conley et al., 2017; Kidder and Mumma, 2003; Sperling et al., 2010). Siliceous radiolarians appeared in the Cambrian, but only diversified and became environmentally significant in the Triassic, and may have further lowered marine silica concentrations (Conley et al., 2017; Wever et al., 2003). Subsequently, siliceous diatoms appeared in the Mesozoic, and their widespread Cenozoic expansion, particularly in the Southern Ocean across the Eocene–Oligocene boundary (Egan et al., 2013), is commonly thought to have decreased marine silica concentrations to modern levels ( $<100 \mu\text{mol.l}^{-1}$  in

deep water) and shifted the locus of siliceous sedimentation to basinal settings (Sims et al., 2006).

Although  $\text{SiO}_2$  was a major constituent of seawater for much of Earth's history, the impact of high silica concentrations on non-silicifying microbes is poorly constrained. Silica is not considered an essential nutrient for non-silicifying microbes, and many species can grow in media with no added silica. However, prokaryotes and eukaryotes clearly evolved and diversified in oceans with dramatically different  $\text{SiO}_2$  compared with today. The presence of elevated  $\text{SiO}_2$  may influence non-silicifying microbes in several ways. For example, if silica accumulates inside the cell, microbes may be unequipped to manage high intracellular  $\text{SiO}_2$  levels. In addition,  $\text{SiO}_2(\text{aq})$  forms aqueous complexes with other dissolved species, which may alter their bio-availability in seawater and potentially also inside the cell, resulting in nutrient limitation. In addition, silica may also be taken up through ion-specific channels designed for chemically similar species, blocking nutrients from entering the cell (Wu and Beitz, 2007). However, if extant species have a genetic memory of ancient high  $\text{SiO}_2$  oceans, they may have cellular machinery to circumvent these potential issues (Marron et al., 2016).

Although previous work has examined the impacts of aqueous silica concentrations on phytoplankton in the range  $1\text{--}100\ \mu\text{mol.l}^{-1}$  (Baines et al., 2012; Brzezinski et al., 2017; Fuhrman et al., 1978), those studies did not extend to the very high silica concentrations thought to be relevant to the Precambrian oceans. Thus, to evaluate responses of major eukaryotic lineages to  $\text{SiO}_2$  addition at high concentration, we grew three chlorophyll *a+c* containing algae ("red lineage") and one chlorophyll *b* containing algae ("green lineage"), including calcifying and non-calcifying strains, under variable  $\text{SiO}_2$  (up to  $2.1\ \text{mmol.l}^{-1}$ ). We

analysed two key functional traits, cell size and growth rates, as well as cellular quotas of phosphorus, silica, and a range of bioessential metals. For comparison with the prokaryotic realm, we also investigated a cyanobacteria species known to accumulate intracellular silica.

## 2. METHODS

### 2.1 Microbe species

All culture strains were acquired from the Roscoff Culture collection (Roscoff, France).

Eukaryote species selected for the study included chlorophyll *b* containing algae (hereafter green lineage), *Chlamydomonas concordia* (strain RCC 1). Three chlorophyll *a+c* containing algae, *Thoracosphaera heimii* (strain RCC 1512), *Pavlova lutheri* (strain RCC 1547) and *Emiliania huxleyi* (strain RCC 1216). Since these strains all acquired their plastids via secondary endosymbiosis from red algae (rhodophytes), they will be referred to hereafter as red lineage. The prokaryote species selected was the *Synechococcus* sp. (strain WH8102/RCC539). The selected group includes species that possess Si specific transporters, such as SITs and related gene families (SIT-Ls and Lsi2), and others that do not. *T. heimii* is a calcifying dinoflagellate and member of the Alveolata division. There is no genome available for *T. heimii*, but other dinoflagellates have SIT-2 and Lsi2-like transporters (Marron et al., 2016). *E. huxleyi* is a calcifying coccolithophore and a member of the Haptophyta division. Some coccolithophore species have SITs, and *E. huxleyi* has Lsi2-like transporters (Durak et al., 2016). *P. lutheri* is a non-calcifying red lineage algae and member of the division haptophyte, and has no reported Si transporters. *C. concordia* is a non-calcifying algae from the green lineage and member of the division chlorophyta. The presence of Si transporters in *C. concordia* is not documented, but closely related *C. reinhardtii* has none.

*Synechococcus* is a globally abundant cyanobacteria previously shown to accumulate intracellular Si, and contains SIT-L genes (Baines et al., 2012; Brzezinski et al., 2017).

## 2.2 Culture conditions

Each species was grown as a batch culture in an artificial seawater media, Aquil\* (Price et al., 1989; Sunda et al., 2005). Aquil\* is enriched with 100  $\mu\text{mol.l}^{-1}$  nitrate and 10  $\mu\text{mol.l}^{-1}$  phosphate, and in equilibrium with modern atmospheric  $\text{CO}_2$ . In the control, silicic acid was not added, but unamended concentrations ranged up to 25  $\mu\text{M}$  due to the presence of trace amounts of silica in other salts (Media A, Table 1). In silica-rich seawater,  $\text{SiO}_2$  was added to achieve concentrations ranging between 1.2 and 2.1  $\text{mmol.l}^{-1}$  from sodium metasilicate stock solutions (media C–E, Table 1).  $\text{SiO}_2$  was added before any nutrients and stirred for >48 hours to ensure the stock solution was fully equilibrated with the media.  $\text{SiO}_2$  was varied between batches of media to test whether there was a progressive response to increases in  $\text{SiO}_2$ . Some cultures were also tested under standard Aquil\* media, with 100  $\mu\text{M}$  of added  $\text{SiO}_2$  (Media B, Table 1). Si concentrations in each batch of media were analysed via inductively coupled plasma optical emission spectroscopy (ICP-OES) at the University of Cambridge. Vitamins and trace metals were added according to the Aquil\* recipe (Price et al., 1989; Sunda et al., 2005). The media was pH balanced to 8.1–8.2 prior to inoculation by the addition of NaOH and HCl. The trace metal chelator EDTA (ethylenediaminetetraacetic acid) was added to the trace metal stock solutions to guarantee a constant level of bioavailable metals and prevent metal precipitation. All stock solutions were added under sterile conditions in a laminar flow hood.

**Table 1:** SiO<sub>2</sub>(aq) concentrations in each batch of media, analysed via ICP-OES. Average error is <5% (1σ).

Media type	SiO <sub>2</sub> (aq)
A	<25 μmol.l <sup>-1</sup>
B	0.1 mmol.l <sup>-1</sup>
C	1.2 mmol.l <sup>-1</sup>
D	1.6 mmol.l <sup>-1</sup>
E	2.1 mmol.l <sup>-1</sup>

All culture bottles were manually and carefully rotated daily to avoid cell settling. The cultures were incubated in a climate chamber at a constant temperature of 15°C for haptophyta and alveolata, and 20°C for dinoflagellates and cyanobacteria, at a 12:12 (hour:hour) light-dark cycle and at a photon flux density of 20 μmol photons m<sup>-2</sup> s<sup>-1</sup> for alveolata and haptophyta and 100 μmol photons m<sup>-2</sup> s<sup>-1</sup> for dinoflagellates and cyanobacteria. All cultures were grown in sterile non-TC treated 100 cm<sup>3</sup> polystyrene culture vessels. All work was undertaken using sterile techniques, and cultures were only opened inside a sterile laminar flow hood and sampled with autoclaved pipette tips. The initial cell density was relatively low, and cells were transferred into fresh media during mid-exponential phase. Each species was grown in triplicate under both silica-rich and control conditions. Some species were also grown in standard Aquil\*+Si media (Media B). The pH of the media was monitored during exponential growth of both *T. heimii* and *E. huxleyi* in silica-rich media as well as a sterile control.

### 2.3 Cell abundance and growth rate

137 Samples for cell abundance were taken at regular intervals throughout lag, exponential and  
138 early stationary phase. Care was taken to sample within the same time interval each day,  
139 and control and Si-rich conditions were sampled within five minutes of each other.  
140 Incubation bottles were agitated to obtain a homogeneous suspension of cells before  
141 sampling. Eukaryote cells were diluted 10-fold with a 3.5% NaCl solution and immediately  
142 measured in triplicate using a Beckman Z1 Coulter counter within a species-specific size  
143 window designed to exclude debris, such as dead cells, bacteria or detached coccoliths. The  
144 Coulter counter was calibrated using spherical beads. Species specific daily growth rates  
145 were calculated from the least-squares regression of cell counts versus time during  
146 exponential growth (Eq).

$$147 \quad \mu = [\ln(c_1) - \ln(c_0)]/[t_1 - t_0].$$

148 Where  $c_0$  and  $c_1$  are the cell concentrations at the beginning ( $t_0$ ) and end ( $t_1$ ) of the  
149 incubation period (for full cell count and cell size data, see supplementary figures S1–S5).  
150 The optimal period for calculating exponential growth was carefully assessed for each sub-  
151 culture, ensuring that the points used remained within the exponential growth phase,  
152 covered several complete photoperiods and excluded data points associated with large error  
153 bars (supplementary figures S1–S5). Growth rates in this study refer to cell division rates,  
154 rather than increased cellular mass. The spherical equivalent diameter of cells was also  
155 measured using a coulter counter, and used to calculate the mean diameter. *T. heimii* and *E.*  
156 *huxleyi* samples were acidified with a few drops of 10 M HCl after analysis, mixed for one  
157 hour, and reanalysed to determine naked cell size after dissolution of calcified shells.  
158  
159 Chlorophyll levels in cyanobacteria cultures were measured in triplicate using a TECAN  
160 spark® Multimode plate reader at an excitation wavelength of 485 nm. Chlorophyll levels

can be assumed to track cell density, but may also be influenced by variations in the pigment content of individual cells within each treatment. For all species, analysis was performed within a one-hour time window daily to minimise the influence of sampling different parts of the daily growth cycles.

## 2.4 Cell imaging

Samples were taken from the *T. heimii* incubation bottles and 2 ml of media was filtered under low vacuum onto polycarbonate filters (0.22 µm pore size) and rinsed five times with 10 mmol.l<sup>-1</sup> CaCl<sub>2</sub> and then five times with 100% ethanol. Filter papers were dried in a laminar flow hood. Samples were gold coated and SEM analysis was performed at the Dunn School of Bioimaging in the Department of Physiology, University of Oxford with a Zeiss Sigma 300 FEG-SEM.

## 2.5 Total digestions

Cells were centrifuged during mid-exponential phase, and washed three times in chelexed metal-free seawater, which had a pH of 8 and contained no added nutrients or Si (SOW). During each wash, the cells were in contact with the SOW for over 20 minutes. Cells were then dried under laminar flow and frozen for > 24 hours. Cell pellets were transferred to clean Teflon beakers under clean lab ISO 100 conditions and digested in a 4:6 mixture of hydrogen peroxide and concentrated nitric acid under reflux for 24 hours. The digests were then dried down and re-suspended in 2% nitric acid for analysis via flow injection ICP-MS (Zhang et al., 2018). The concentration of metals in the media was also analysed via ICP-MS. Si was measured on the same digests via ICP-OES at the University of Cambridge. Cellular element concentrations were calculated based on the total number of cells and the average



cell volume, as measured on a Coulter counter (See section 2.3). These bulk cellular digests are reflect intracellular concentrations, but will also include contributions from any species precipitated on or adsorbed to the exterior cell wall.

### 3. RESULTS

#### 3.1 Growth rates and cell diameter

Consistently reduced growth rates were observed in *T. heimii*, *C. concordia* and *P. lutheri* in silica-rich seawater compared with the control (Figure 2). These differences were statistically significant as determined by a one-way ANOVA test (supplementary figure S6 and table 2). In contrast, there was no consistent difference in growth rate for *E. huxleyi* or *Synechococcus sp.* between the high-silica treatment (Media C–E) and the control (Media A, no added SiO<sub>2</sub>) (Figure 2). For algae grown under intermediate-SiO<sub>2</sub> seawater (Media B = 100 µmol.l<sup>-1</sup> SiO<sub>2</sub>), there was no significant difference in growth rates compared with the control (Media A). The pH remained within error of sterile media during early and mid-exponential phase, but started to rise in late exponential phase once cell densities reached >10<sup>5</sup> ml<sup>-1</sup>, reaching 8.4 by stationary phase (figure SX).

Another striking difference between the high Si treatment (Media C–E) and the control (Media A) was reduced average cell diameter at maximum growth rates, observed in *T. heimii*, *E. huxleyi*, and *P. lutheri* (at the P < 0.05 level, see figure 2 and table 2). The cell size difference persisted in *T. heimii* and *E. huxleyi* after acidification, suggesting a true difference in the size of the naked cell, rather than a change in calcification (See supplementary figure S7). There was no consistent difference in cell diameter observed in *C. concordia*, and no cell size data are available for *Synechococcus sp.* The reduced diameter

translates into a dramatically reduced surface area and cell volume, but increases the surface area to volume ratio. In summary, all algal species showed some **systematic response to** of elevated SiO<sub>2</sub>, via reduced growth rates and/or cell size, except for the cyanobacterial species, *Synechococcus sp.*

**Table 2:** Average growth rates and cell size at maximum growth rate for Si-rich and control experiments across all sub-cultures. Error is one standard deviation. Results of one-way Anova test for high-silica treatments compared with control for each subculture. P <0.05 suggests the difference between the means of the two groups is statistically significant. The F statistic [F(B,W)=R] states the degrees of freedom between (B) and within (W) each group, respectively, which is used to calculate the F ratio (R).

Species	Mean growth rate			Mean cell size		
	high-Si	control	One way Anova test	high-Si	control	One way Anova test
<i>C. concordia</i>	0.15 ± 0.05	0.20 ± 0.04	F(1,16)=6.72, p=0.02	5.56 ± 0.57	5.94 ± 0.41	F(1,16)=2.67, p=0.122
<i>T. heimii</i>	0.31 ± 0.18	0.58 ± 0.26	F(1,28)=11.28, p=0.00	10.42 ± 0.53	11.02 ± 0.58	F(1,28)=8.89, p=0.006
<i>P. lutheri</i>	0.16 ± 0.03	0.17 ± 0.03	F(1,10)=82.93, p=0.00	4.48 ± 0.04	4.68 ± 0.07	F(1,10)=42.44, p=0.000
<i>E. huxleyi</i>	0.76 ± 0.11	0.78 ± 0.12	F(1,52)=0.25, p=0.62	4.81 ± 0.18	5.10 ± 0.16	F(1,52)=42.21, p=0.000

<i>Synechococcus</i>	0.31 ±	0.30 ±	F(1,40)=0.01,	N/A	N/A	N/A
<i>sp.</i>	0.22	0.20	p=0.93			

### 3.2 Cellular composition

In general, eukaryotic metal quotas for Fe, Mn, Br and Zn are high compared with Co, Cd, Cu, I, Mo, Zr, Ba, Cr and Se, in agreement with the less expansive previous cellular metal quotas reported in Quigg et al., (2003) (See supplementary discussion). There is a small but progressive increase in the intracellular concentration of Se, Mo and Ba at higher silica concentrations for *T. heimii* (Figure 3), and a larger increase in the concentration of intracellular As, Al and Zr. Similarly, the cellular concentration of Mo, Ba, Al and As is significantly higher in *C. concordia* cells grown in silica-rich seawater compared with a control (Figure 3). For *P. lutheri*, the cellular concentration of Al and Ge is higher in silica-rich conditions compared to the control (Figure 3). Other metals show no change outside of error (1 SD) between the control and silica-rich conditions. These patterns cannot be explained by different concentrations of metal in the sterile media (see Figure S9 in the supplementary information). In summary, for most bio-essential metals, elevated SiO<sub>2</sub>(aq) does not appear to influence cellular metal quotas, but there is an increase in the intracellular concentration of some toxic metalloids.

*T. heimii*, *E. huxleyi*, *C. concordia* and *P. lutheri* all accumulate intracellular silica at concentrations orders of magnitude higher than the media. All species show an increase in intracellular silica concentration when grown in silica-rich media, and this is most pronounced in *T. heimii* and *E. huxleyi*, where intracellular silica concentrations exceed 200 mmol.l<sup>-1</sup> (Figure 4). Enrichment factors (the ratio of silica in the cell to silica in the media)

242 remain within an order of magnitude for most individual sub-cultures across a range of  
 243  $\text{SiO}_2(aq)$ , despite large variation between species and subcultures. *C. concordia* shows a  
 244 different enrichment factor between two sub-cultures, with lower intracellular Si when the  
 245 cells were harvested later in exponential phase, suggesting that silica accumulation rates are  
 246 highest at the start of exponential phase and decline during growth. For *T. heimii*,  
 247 intracellular P concentrations also increased under silica-rich conditions (Figure 4).

248

249 **Table 3:** Summary of response to silica-rich seawater compared to a control. Presence or  
 250 absence of **silica specific transporters** as reported in Durak et al., (2016) and Marron et al.,  
 251 (2016).

	Species	Lineage	Calcifying?	Silicon transporters	Growth rates under high Si treatment c.f. control	Cell diameter under high Si treatment c.f. control
Eukaryotes	<i>E. huxleyi</i>	Red	Yes	Lsi2-like	Same	Lower
	<i>T. heimii</i>	Red	Yes	Unknown, <b>but</b> <b>other</b> dinoflagellates have SIT-L & Lsi2-like.	Lower	Lower
	<i>C. concordia</i>	Green	No	Unknown, <b>but</b> <b>closely related</b>	Lower	Same

				<i>C. reinhardtii</i> has none.		
	<i>P. lutheri</i>	Red	No	None reported	Lower	Lower
Prokaryote	<i>Synechococcus</i> <i>sp.</i>	N/A	No	SIT-L	Same	N/A

252

### 253 3.3 SEM data

254 During **dinoflagellate** cell division, the cell temporarily enters a resting stage, and then the  
255 daughter cell emerges through the excystment opening. The excystment opening was  
256 clearly visible in around a third of calcified *T. heimii* cells grown under control conditions,  
257 but none were observed in cells grown under Si-rich conditions (Figure 6), despite observing  
258 >50 individual cells. Aside from this, there were no other observable differences in surface  
259 texture or morphology between cells grown under control and Si-rich conditions, including  
260 no evidence of extracellular SiO<sub>2</sub> precipitates.

261

## 262 4. DISCUSSION

### 263 4.1 Eukaryotic stress in silica-rich seawater

264 All eukaryotic algae investigated here show **potential** signs of stress, including smaller cell  
265 size and/or reduced maximum growth rates under elevated SiO<sub>2</sub>(aq). This observation is  
266 consistent across the major eukaryotic lineages examined here, including algae from red  
267 and green lineages, and calcifying and non-calcifying red lineage algae. Relative to controls  
268 (i.e., no added SiO<sub>2</sub>(aq)), low concentrations of silica (up to 100 µmol.l<sup>-1</sup>) resulted in no  
269 discernible influence on growth rates, consistent with previous studies that tested silica

270 levels between 1 and 100  $\mu\text{mol.l}^{-1}$  (Fuhrman et al., 1978). However, silica appears to  
271 become detrimental to eukaryotic algae between 100  $\mu\text{mol.l}^{-1}$  and 1  $\text{mmol.l}^{-1}$ ,  
272 concentrations higher than any region of the modern ocean ( $<100 \mu\text{mol.l}^{-1}$  in deep waters,  
273 but as low as  $<0.2 \mu\text{mol.l}^{-1}$  in surface waters). Beyond these concentrations, increasing  $\text{SiO}_2$   
274 (between 1.2 and 2.1  $\text{mmol.l}^{-1}$ ) resulted in no discernible additional change in growth rates.  
275 In addition to changes in growth rate, all three algae from the red lineage show reduced cell  
276 sizes under high-Si treatment. Reduced cellular growth rate and/or cell size are common  
277 indicators of stress in algal culture. The absence of visible excystment openings in  
278 dinoflagellates grown under high-Si conditions is also consistent with slower cell division  
279 rates under stress. We will explore three possible mechanisms for inducing stress under  
280 high-Si conditions, including nutrient limitation, metal toxicity, and the direct effects of  
281 intracellular Si accumulation.

282

## 283 4.2 Nutrient limitation

284 Reduced growth rates are a common response to nutrient limitation. As we shall explore,  
285 nitrate limitation, rather than phosphate, is more likely the principal driver of both reduced  
286 growth rates and reduced cell size. In the exponential growth phase, the mean diameter in a  
287 population of cells is controlled by the rate of nutrient assimilation into biomass and the  
288 time interval between cell division (i.e., the generation time) (Aloisi, 2015). In the  
289 assimilation phase of the cell cycle,  $\text{NO}_3^-$  consumption is higher as cells synthesize and  
290 accumulate biomass. Immediately before cell division, phosphate consumption is higher, as  
291 cells synthesise nucleic acids and membrane phospholipids. Therefore, phosphate limitation  
292 can arrest the cells in assimilation phase, causing them to bloat to larger sizes before each  
293 cell division. Given that two of the species exhibiting longer generation times (i.e., reduced

294 growth rates) also exhibit reduced cell diameters, this is inconsistent with phosphate  
295 limitation. Further, the enhanced accumulation of P in *T. heimii* under silica-rich conditions  
296 is inconsistent with P limitation (figure 4), and instead suggests *T. heimii* continues to  
297 accumulate P as some other factor limits growth rates. In contrast,  $\text{NO}_3^-$  limitation results in  
298 reduced cell diameter at each division, and so could explain the combination of longer  
299 generation times and reduced cell diameter observed in *T. heimii* and *P. lutheri* in Si-rich  
300 seawater. This could occur if high  $\text{SiO}_2(\text{aq})$  indirectly affects nitrate bioavailability in  
301 seawater, blocks nitrate uptake pathways, or affects the availability of a micronutrient that  
302 plays a role in nitrate assimilation.

303

304 It is also possible that an alternative micro-nutrient is causing cell stress.  $\text{SiO}_2(\text{aq})$  forms  
305 aqueous complexes with transition metals in seawater solutions that may alter their  
306 bioavailability, in particular if intracellular pH increases, as metal-silicate complex formation  
307 is strongly pH dependent (Choppin et al., 2011). One physiological response to nutrient  
308 limitation is to use an alternative pathway that depends on a different metal, but if a  
309 particular protein site depends on a single metal, an increase in the efficiency of metal  
310 uptake is required to maintain a requisite metabolic rate (Dupont et al., 2010). A reduction  
311 in cell diameter may balance this requirement, since this dramatically increases the surface  
312 area to volume ratio. The reduced cell sizes observed in all three algae from the red lineage  
313 may therefore be an expression of micronutrient limitation.

314

315 Although the intracellular metal concentrations do not show a reduction under the high-Si  
316 treatment (figure 3), metal limitation may not be expressed if the cells physiologically buffer  
317 the “free” metal availability with a storage strategy to maintain constant intracellular free

levels. It is therefore difficult, at present, to identify the ultimate limiting nutrient from cell digests. However, a potential mechanism to reconcile the differential impact of high-Si conditions on eukaryotes and prokaryotes is if high-Si conditions result in Zn and Cu limitation, since eukaryotes have particularly high requirements for these two metals compared to the prokaryotes (Williams and Rickaby, 2012). At high intracellular  $\text{SiO}_2(\text{aq})$  concentrations, Zn and Cu may be complexed with aqueous  $\text{SiO}_2$ , or precipitate as Zn-silicate or Cu-silicate minerals. Available geochemical data suggest that precipitation of Zn- and Cu-silicate minerals should proceed at near neutral pH under the intracellular  $\text{SiO}_2$  concentrations observed here (Tiller and Pickering, 1974; Yates et al., 1998).

#### 4.3 Metal toxicity

Our data suggest that cellular metal quotas increase for some metals in the high-Si treatment. These are largely metals with no known biological role, including As, Al and Ge, but also include Mo, which is required by all microbes. Assuming these metal quotas represent intracellular accumulation, as opposed to adsorption or precipitation on the surface of the cell, they could be a symptom of cell stress: if a critical metal is limited, the stressed algae may respond by indiscriminately taking up other metals from seawater. Alternatively, metalloid accumulation could be a driver of cell stress, if increased metal accumulation is inadvertent. This could occur if the metals are complexed with Si as it enters the cell. Aluminium, for example, forms particularly strong complexes with Si. Some Si specific transporters (e.g.,  $\text{LiS2}$ ) can also transport metalloids, such as arsenic (Ma et al., 2008) or germanium (Durak et al., 2016). Another possibility is that the cells could lose the ability to remove toxic metals under high-Si conditions. The high concentration of Si may compete with metals such as Ge and Al at the efflux pump due to molecular mimicry,



causing build-up of these metals within the cell (Thamatrakoln and Hildebrand, 2008).

Metalloids may also become trapped inside the cell complexed together with the Si, either within metalloid-Si complexes or as an impurity in silicate minerals. Regardless of the accumulation mechanism, high metalloid contents are a sign of stress and could result in intracellular metal toxicity.

#### 4.4 Intracellular silica accumulation

Free Si in the cytoplasm has the potential to catastrophically disrupt cellular metabolism, by, for example, binding to proteins (Bienert et al., 2008). The eukaryote species tested here were all found to accumulate intracellular silica in the control ranging from 3–17 mmol.l<sup>-1</sup>. Intracellular SiO<sub>2</sub> accumulation in eukaryotes appears to scale with the SiO<sub>2</sub> concentration in the media. Therefore, in the high SiO<sub>2</sub> treatment, intracellular SiO<sub>2</sub> levels were much higher, ranging from ~20 mmol.l<sup>-1</sup> in *P. lutheri* to ~400 mmol.l<sup>-1</sup> in *E. huxleyi*. Silica begins to auto-polymerise at concentrations >2 mmol.l<sup>-1</sup> under circumneutral pH (Iler, 1979), and so these intracellular silica concentrations range up to 200 times above silica saturation (Siever, 1962; Siever and Woodford, 1973). This phenomenon has been noted previously in microbes including *Synechococcus sp.*, *Platymonas sp.* and *Phaeodactylum tricornutum* (Baines et al., 2012; Brzezinski et al., 2017; Fuhrman et al., 1978; Nelson et al., 1984), and the intracellular SiO<sub>2</sub> concentrations fall within a similar range, despite a range of culturing and SiO<sub>2</sub> analysis techniques, suggesting intracellular silica accumulation is widespread among non-silicifying microbes (Figure 5).

One concern is that the bulk cellular digests included inorganic phases such as Mg-silicates that precipitated on cell surfaces or as an independent phase in the media, and were not

366 removed during washing. Mg-silicate precipitation is favoured at higher pH (>8.5) (Tutolo  
367 and Tosca, 2018). Although the media was set to pH 8.1–8.2 before inoculation, pH **can**  
368 increase in dense batch cultures due to photosynthetic CO<sub>2</sub> uptake, **potentially** reaching pH  
369 >8.5 (Nelson et al., 1984). However, **several** observations rule out inorganic Mg-silicate  
370 **contributions to our bulk digests**. First, apparent silica uptake in *C. concordia* is higher in the  
371 early stages of exponential phase, when the pH change is likely to be small (**Figure 4**).  
372 Second, silica accumulation is observed in **both** calcifying **and non-calcifying** species, despite  
373 calcification driving a decrease in pH throughout growth that **could** counterbalance the pH  
374 increase driven by photosynthesis (Nimer et al., 1994). **We confirmed that the pH remained**  
375 **within range of a sterile control during early and mid-exponential phase for both *T. heimii***  
376 **and *E. huxleyi* in silica-rich media (figure SX). Since we harvested cells in mid-exponential**  
377 **phase, this rules out the possibility of pH induced precipitation**. Third, the cells were **soaked**  
378 three times in SOW with a pH of 8 prior to digestion, which should have dissolved any  
379 inorganic Mg-silicates (Nelson et al., 1984). Therefore, our data support true intra- or extra-  
380 cellular organic uptake/absorption of silica by all four species, consistent with previous  
381 reports of intracellular silica accumulation in non-silicifying microbes at similar levels (Figure  
382 5; Baines et al., 2012; Brzezinski et al., 2017; D’Elia et al., 1979; Fuhrman et al., 1978).

383

384 What form does this cellular silica take? One possibility is that silicate minerals **were**  
385 **deposited** external to the cell wall. However, no evidence for this was observed with our  
386 SEM images of *T. heimii*, in cells associated with significant Si accumulation (Figure 6).  
387 Observations of intracellular silica accumulation in *Synechococcus* in the open ocean, where  
388 ambient SiO<sub>2</sub>(aq) is undersaturated with respect to silicate minerals, further supports a true  
389 intracellular form (Baines et al., 2012). If the SiO<sub>2</sub> present in bulk cell digests is truly

intracellular, it is possible that silicate minerals are precipitating inside the cell, contained within membrane bound vacuoles, although no such vacuoles have been observed in diatom studies (Rogerson et al., 1987). An alternative possibility for maintaining such high intracellular silica concentrations is the presence of organic complexes inside the cell that bind to silica and increase its solubility (Hildebrand, 2000; Hildebrand and Wetherbee, 2003; Martin-Jézéquel et al., 2000). There is currently no direct evidence for such complexes existing outside of diatoms, and they remain poorly characterised (Azam, 1974; Baines et al., 2012; Bhattacharyya and Volcani, 1983; Hildebrand, 2000; Sullivan, 1979).

398

Such high intracellular silica concentrations raise the question of how silica is entering and being retained within the cell. If silica is acting as a nutrient, then it may be entering the cell via active uptake. The algae tested here grow faster in low-silica seawater, suggesting Si is not an essential nutrient. However, active Si uptake may be a strategy to lower local seawater Si to inhibit silica-dependent competitors (Fuhrman et al., 1978), and small amounts of silica have been shown to play an indirect role in other processes, such as coccolith formation (Durak et al., 2016). Active transport of Si into and around the cell could be facilitated by silica specific transporters, such as the SITs, a gene family first characterised in diatoms that facilitate  $\text{Na}^+$  coupled transport of silicic acid (Hildebrand et al., 1997). SITs are present in diatoms, where they are required to move Si around the cell to the silica depositional vesicle without inducing polymerisation. Recent work has found that SITs and related gene families (SIT-Ls and Lsi2) are present across a broad range of species from disparate lineages, including non-silicifying taxa, and appear to have a common origin (Durak et al., 2016; Marron et al., 2016). If algae have a form of Si importer that is constitutively expressed, and no regulatory pathway to switch the transporter off in high-

414 silica environments, then in the absence of an independent and efficient efflux pathway,  
415 cells could continue to accumulate intracellular silica.  
416

417 However, Si accumulation and signs of stress occur in species both with and without known  
418 Si transporters (Table 3). *E. huxleyi* has Lsi2-like Si transporters, and *Synechococcus*  
419 possesses SIT-L genes (Marron et al., 2016). Some dinoflagellates have SIT-L and Lsi2  
420 transporters, but phylogenetic analysis is required to confirm whether they are also present  
421 in *T. heimii*. In contrast, the presence of Si transporters in *C. reinhardtii* and *P. lutheri* is not  
422 documented. Thus, even species with Si transporters, which may help safely transport silica  
423 around the cell, are overloaded when  $\text{SiO}_2(\text{aq})$  reaches Precambrian levels ( $>1 \text{ mmol.l}^{-1}$ ).  
424 This is consistent with the high binding affinity for SITs ( $K_D=2.9 \text{ }\mu\text{M}$ ) (Knight et al., 2016). The  
425 presence of high intracellular silica levels in species without known Si transporters suggests  
426 that Si uptake may not be exclusively occurring via Si-specific transporters. Further, it  
427 suggests that the presence of Si transporters is not able to regulate intracellular Si  
428 accumulation through increased efflux, either because they are not adapted for efflux in  
429 extant species, or because the efflux pathways are also overwhelmed at such high ambient  
430  $\text{SiO}_2(\text{aq})$ .  
431

432 Another possibility is that active uptake is occurring mistakenly, via transporters intended  
433 for other ions. This could result in nutrient starvation if Si interferes with the uptake  
434 efficiency of other transporters. Alternatively, uncharged forms of silica may be entering the  
435 cell via diffusion. There appears to be a species-specific proportional relationship between  
436 intracellular  $\text{SiO}_2$  levels and the concentration of  $\text{SiO}_2$  in the media, suggesting they have  
437 very little control over uptake, consistent with diffusion (Figure 4). Diffusion could continue

across the cell wall, despite intracellular concentrations exceeding ambient marine  $\text{SiO}_2(aq)$ , if organic complexes are present that bind to intracellular silica, increasing its solubility (Thamatrakoln and Hildebrand, 2008).

#### **4.5 Early eukaryotes, intracellular $\text{SiO}_2(aq)$ uptake, and Precambrian $\text{SiO}_2(aq)$ levels**

The first unambiguous eukaryotic fossils are found in the late Palaeoproterozoic era ( $>1.65$  Ga), but eukaryotes remained ecologically marginalised throughout the Mesoproterozoic (Butterfield, 2015; Javaux, 2007; Javaux et al., 2001; Javaux and Knoll, 2017; Javaux and Lepot, 2018). Recent data indicate that eukaryotic microfossils increase in taxonomic richness during and after the  $\sim 800\text{--}780$  Ma Bitter Springs Event, but this metric progressively decreases leading up to the  $\sim 717$  Ma onset of the Sturtian glaciation (Cohen and Riedman, 2018; Riedman and Sadler, 2018). Biomarker data have been interpreted to reflect a rise to ecological dominance in the aftermath of the Sturtian glaciation, at which point eukaryotic contributions to organic carbon remain significant through much of the remaining Neoproterozoic (Figure 1) (Brocks et al., 2017; Cohen and Macdonald, 2015). From one perspective, these data indicate that early eukaryotic diversification took place in oceans that featured higher levels of  $\text{SiO}_2(aq)$  than today, simply because these evolutionary events pre-date the radiation of siliceous skeletons in the Phanerozoic (Siever, 1992; Sperling et al., 2010). At the same time, our culturing data suggest that elevated  $\text{SiO}_2(aq)$  levels have a negative physiological effect on a range of extant eukaryotes. Did marine  $\text{SiO}_2(aq)$  levels influence Proterozoic eukaryotic ecosystems, and if so, how?

Although **Si transporters such as SITs** currently play a role in uptake and transport **across many eukaryote species**, it has been proposed that the original role of **Si transporters** was

462 for silica detoxification in high-Si Precambrian oceans (Marron et al., 2016). In the early  
463 Palaeozoic, these transporters may have been adapted for biosilicification as part of an  
464 evolutionary arms race that included the appearance of biominerals made from carbonate,  
465 phosphate and silicate minerals (Marin et al., 1996). This in turn reduced ambient marine  
466  $\text{SiO}_2(aq)$  levels (Maliva et al., 1989), driving widespread loss or transformation of Si  
467 transporters in non-silicifying species (Marron et al., 2016). This hypothesis implies that in  
468 Precambrian oceans, microbes would have had biochemical machinery to deal with elevated  
469 marine  $\text{SiO}_2(aq)$ . In contrast, our results suggest that where Si transporters were retained,  
470 those species still struggle to deal with elevated  $\text{SiO}_2(aq)$  ( $>1 \text{ mmol.l}^{-1}$ ). However, this may  
471 simply indicate that Si transporters in extant organisms have been adapted to new  
472 conditions, by changing their role or binding affinity, and can no longer act as efficient efflux  
473 pumps under very high  $\text{SiO}_2(aq)$ . If early eukaryotes did lack specialist adaptations to cope  
474 with elevated  $\text{SiO}_2(aq)$ , then the abundance of diverse eukaryotes in late Proterozoic  
475 ecosystems could indicate that  $\text{SiO}_2(aq)$  was lower or more variable than commonly  
476 thought.

477

478 A critical issue in determining how marine  $\text{SiO}_2(aq)$  levels influenced early eukaryotic  
479 ecosystems is to what extent the record of syngenetic and early diagenetic chert  
480 actually constrains marine  $\text{SiO}_2(aq)$  concentrations. Although primary silica grains  
481 characterise many Archean and Palaeoproterozoic successions, evidence for direct  
482 amorphous silica primary precipitation from the water column in the later Proterozoic is in  
483 fact more limited. Silica-rich granules clearly attest to spontaneous precipitation of  
484 amorphous  $\text{SiO}_2$  from the water column in the Archean, indicating that seawater  
485 occasionally crossed solubility requirements, perhaps with the help of salinity fluctuations

(Stefurak et al., 2015, 2014). Similarly, many silica-rich facies within banded iron formations contain evidence for primary or early diagenetic silica precipitation in subtidal environments (Maliva et al., 2005; Rasmussen et al., 2015). In contrast, most early diagenetic chert of late Proterozoic age formed in peritidal settings, and is petrographically distinct in comparison (Fairchild et al., 1991; Hofmann, 1976; Knoll, 1982; Knoll et al., 1991; Muir, 1976; Schopf, 1968; Sergeev et al., 1997, 1995). For example, early silicification of carbonate-rich lithologies includes permineralisation of organic matter, chalcedonic cements, micro-quartz precipitation as carbonate minerals were replaced, and mosaics of larger interlocking quartz crystals somewhat similar to “mesoquartz” produced from modern silica sinters (Green et al., 1989; Knoll, 1985; Knoll and Simonson, 1981; Maliva et al., 2005, 1989).

Although permineralisation must have occurred very soon after organic material entered the sediments (i.e., before complete degradation), the marine  $\text{SiO}_2(aq)$  concentrations required to drive this process are poorly constrained. On the basis of sedimentological and stratigraphic constraints, many authors have suggested that evaporation in peritidal settings assisted in driving early silicification (Fairchild et al., 1991). Because early diagenetic silicification is comparatively rare in sediments today, these data imply elevated  $\text{SiO}_2(aq)$  levels compared with the modern ocean. This inference is also supported by recent experimental data showing that the formation and subsequent breakdown of aqueous organo-silica complexes facilitates high supersaturation and rapid nucleation of amorphous silica from seawater-like solutions (Escario et al., 2020). Nevertheless,  $\text{SiO}_2(aq)$  could potentially have been below amorphous silica saturation, or even cristobalite saturation, through much of the late Proterozoic. In fact, mass balance modelling of the chert-hosted  $\delta^{30}\text{Si}$  record suggests that marine  $\text{SiO}_2(aq)$  might have decreased through the later portion

of the Proterozoic compared to earlier intervals (Figure 1; Trower and Fischer, 2019), possibly driven by increases in authigenic clay formation (Isson and Planavsky, 2018). Thus, disentangling the relationship between early eukaryotic evolution and the history of marine  $\text{SiO}_2(\text{aq})$  requires improved and more quantitative estimates of marine  $\text{SiO}_2(\text{aq})$  through time, and a more complete understanding of the physiological mechanisms underpinning metabolic activities of early eukaryotes in  $\text{SiO}_2(\text{aq})$ -rich seas.

## 5. CONCLUSIONS

When exposed to Si-rich solutions that mimic Archean–Proterozoic seawater, extant eukaryotic algae show signs of physiological stress. Under these conditions, eukaryotic algae accumulate intracellular silica, reaching concentrations far above the saturation state of common silicate minerals, regardless of whether they possess silica specific transporters. Such high levels of intracellular silica could interfere with normal cellular metabolism by, for example, chelating bioessential metals or trapping toxic metalloids. Early eukaryotes may have possessed modified **Si transporters**, designed to pump silica out of the cell, as an adaptation to Si-rich oceans. Alternatively, silica concentrations during early eukaryotic evolution may have been lower or more variable than commonly thought. One major outstanding question is why prokaryotes do not show signs of stress under elevated  $\text{SiO}_2(\text{aq})$ , despite accumulating intracellular silica at comparable concentrations. This raises some interesting questions about the physiological mechanism underpinning the stress response in eukaryotes, with important implications for understanding the influence of declining  $\text{SiO}_2(\text{aq})$  on early microbial evolution.

## REFERENCES



534 Aloisi, G., 2015. Covariation of metabolic rates and cell size in coccolithophores.  
 535 Biogeosciences 12, 6215–6284. <https://doi.org/10.5194/bg-12-4665-2015>  
 536 Azam, F., 1974. Silicic-acid uptake in diatoms studied with [68Ge]germanic acid as tracer.  
 537 Planta 121, 205–212. <https://doi.org/10.1007/BF00389321>  
 538 Baines, S.B., Twining, B.S., Brzezinski, M.A., Krause, J.W., Vogt, S., Assael, D., McDaniel, H.,  
 539 2012. Significant silicon accumulation by marine picocyanobacteria. Nat. Geosci. 5,  
 540 886–891. <https://doi.org/10.1038/ngeo1641>  
 541 Bhattacharyya, P., Volcani, B.E., 1983. Isolation of silicate ionophore(s) from the  
 542 apochlorotic diatom *Nitzschia alba*. Biochem. Biophys. Res. Commun. 114, 365–372.  
 543 [https://doi.org/10.1016/0006-291X\(83\)91636-4](https://doi.org/10.1016/0006-291X(83)91636-4)  
 544 Bienert, G.P., Schüssler, M.D., Jahn, T.P., 2008. Metalloids: essential, beneficial or toxic?  
 545 Major intrinsic proteins sort it out. Trends Biochem. Sci. 33, 20–26.  
 546 <https://doi.org/10.1016/j.tibs.2007.10.004>  
 547 Brocks, J.J., Jarrett, A.J.M., Sirantoine, E., Hallmann, C., Hoshino, Y., Liyanage, T., 2017. The  
 548 rise of algae in Cryogenian oceans and the emergence of animals. Nature 548, 578.  
 549 <https://doi.org/10.1038/nature23457>  
 550 Brzezinski, M.A., Krause, J.W., Baines, S.B., Collier, J.L., Ohnemus, D.C., Twining, B.S., 2017.  
 551 Patterns and regulation of silicon accumulation in *Synechococcus* spp. J. Phycol. 53,  
 552 746–761. <https://doi.org/10.1111/jpy.12545>  
 553 Butterfield, N.J., 2015. Early evolution of the Eukaryota. Palaeontology 58, 5–17.  
 554 <https://doi.org/10.1111/pala.12139>  
 555 Choppin, G.R., Pathak, P., Thakur, P., 2011. Polymerization and Complexation Behavior of  
 556 Silicic Acid: A Review. Main Group Met. Chem. 31, 53–72.  
 557 <https://doi.org/10.1515/MGMC.2008.31.1-2.53>  
 558 Cohen, P.A., Macdonald, F.A., 2015. The Proterozoic Record of Eukaryotes. Paleobiology 41,  
 559 610–632. <https://doi.org/10.1017/pab.2015.25>  
 560 Cohen, P.A., Riedman, L.A., 2018. It's a protist-eat-protist world: recalcitrance, predation,  
 561 and evolution in the Tonian–Cryogenian ocean. Emerg. Top. Life Sci. 2, 173–180.  
 562 <https://doi.org/10.1042/ETLS20170145>  
 563 Conley, D.J., Frings, P.J., Fontorbe, G., Clymans, W., Stadmark, J., Hendry, K.R., Marron, A.O.,  
 564 Rocha, D.L., L, C., 2017. Biosilicification Drives a Decline of Dissolved Si in the Oceans  
 565 through Geologic Time. Front. Mar. Sci. 4.  
 566 <https://doi.org/10.3389/fmars.2017.00397>  
 567 D'Elia, C.F., Guillard, R.R.L., Nelson, D.M., 1979. Growth and competition of the marine  
 568 diatoms *Phaeodactylum tricornutum* and *Thalassiosira pseudonana*. I. Nutrient  
 569 effects. Mar. Biol. 50, 305–312. <https://doi.org/10.1007/BF00387007>  
 570 Dupont, C.L., Butcher, A., Valas, R.E., Bourne, P.E., Caetano-Anollés, G., 2010. History of  
 571 biological metal utilization inferred through phylogenomic analysis of protein  
 572 structures. Proc. Natl. Acad. Sci. 107, 10567–10572.  
 573 <https://doi.org/10.1073/pnas.0912491107>  
 574 Durak, G.M., Taylor, A.R., Walker, C.E., Probert, I., Vargas, C. de, Audic, S., Schroeder, D.,  
 575 Brownlee, C., Wheeler, G.L., 2016. A role for diatom-like silicon transporters in  
 576 calcifying coccolithophores. Nat. Commun. 7, 10543.  
 577 <https://doi.org/10.1038/ncomms10543>  
 578 Egan, K.E., Rickaby, R.E.M., Hendry, K.R., Halliday, A.N., 2013. Opening the gateways for  
 579 diatoms primes Earth for Antarctic glaciation. Earth Planet. Sci. Lett. 375, 34–43.  
 580 <https://doi.org/10.1016/j.epsl.2013.04.030>

- Fairchild, I.J., Knoll, A.H., Swett, K., 1991. Coastal lithofacies and biofacies associated with syndepositional dolomitization and silicification (Draken Formation, Upper Riphean, Svalbard). *Precambrian Res.* 53, 165–197. [https://doi.org/10.1016/0301-9268\(91\)90071-H](https://doi.org/10.1016/0301-9268(91)90071-H)
- Fuhrman, J.A., Chisholm, S.W., Guillard, R.R.L., 1978. Marine alga *Platymonas* sp. accumulates silicon without apparent requirement. *Nature* 272, 244–246. <https://doi.org/10.1038/272244a0>
- Green, J.W., Knoll, A.H., Swett, K., 1989. Microfossils from silicified stromatolitic carbonates of the Upper Proterozoic Limestone-Dolomite “Series”, central East Greenland. *Geol. Mag.* 126, 567–585. <https://doi.org/10.1017/S0016756800022858>
- Hildebrand, M., 2000. Silicic Acid Transport and its Control During Cell Wall Silicification in Diatoms. *Biominer. Prog. Biol. Mol. Biol. Appl.*
- Hildebrand, M., Volcani, B.E., Gassmann, W., Schroeder, J.I., 1997. A gene family of silicon transporters. *Nature* 385, 688–689. <https://doi.org/10.1038/385688b0>
- Hildebrand, M., Wetherbee, R., 2003. Components and Control of Silicification in Diatoms, in: Müller, W.E.G. (Ed.), *Silicon Biomineralization: Biology — Biochemistry — Molecular Biology — Biotechnology*, Progress in Molecular and Subcellular Biology. Springer, Berlin, Heidelberg, pp. 11–57. [https://doi.org/10.1007/978-3-642-55486-5\\_2](https://doi.org/10.1007/978-3-642-55486-5_2)
- Hofmann, H.J., 1976. Precambrian Microflora, Belcher Islands, Canada: Significance and Systematics. *J. Paleontol.* 50, 1040–1073.
- Iler, K., 1979. The Chemistry of Silica. *Solubility Polym. Colloid Surf. Prop. Biochem. Silica.*
- Isson, T.T., Planavsky, N.J., 2018. Reverse weathering as a long-term stabilizer of marine pH and planetary climate. *Nature* 560, 471–475. <https://doi.org/10.1038/s41586-018-0408-4>
- Javaux, E.J., 2007. The Early Eukaryotic Fossil Record, in: *Eukaryotic Membranes and Cytoskeleton: Origins and Evolution*, Advances in Experimental Medicine and Biology. Springer, New York, NY, pp. 1–19. [https://doi.org/10.1007/978-0-387-74021-8\\_1](https://doi.org/10.1007/978-0-387-74021-8_1)
- Javaux, E.J., Knoll, A.H., 2017. Micropaleontology of the lower Mesoproterozoic Roper Group, Australia, and implications for early eukaryotic evolution. *J. Paleontol.* 91, 199–229. <https://doi.org/10.1017/jpa.2016.124>
- Javaux, E.J., Knoll, A.H., Walter, M.R., 2001. Morphological and ecological complexity in early eukaryotic ecosystems. *Nature* 412, 66–69. <https://doi.org/10.1038/35083562>
- Javaux, E.J., Lepot, K., 2018. The Paleoproterozoic fossil record: Implications for the evolution of the biosphere during Earth’s middle-age. *Earth-Sci. Rev.* 176, 68–86. <https://doi.org/10.1016/j.earscirev.2017.10.001>
- Kidder, D.L., Mumma, S.A., 2003. Silica-replaced oolites, bedded shelf cherts and Paleozoic changes in the silica cycle. *Sediment. Geol.* 162, 159–166. [https://doi.org/10.1016/S0037-0738\(03\)00195-7](https://doi.org/10.1016/S0037-0738(03)00195-7)
- Knight, M.J., Senior, L., Nancolas, B., Ratcliffe, S., Curnow, P., 2016. Direct evidence of the molecular basis for biological silicon transport. *Nat. Commun.* 7, 11926. <https://doi.org/10.1038/ncomms11926>
- Knoll, A.H., 1985. Exceptional preservation of photosynthetic organisms in silicified carbonates and silicified peats. *Phil Trans R Soc Lond B* 311, 111–122. <https://doi.org/10.1098/rstb.1985.0143>

Knoll, A.H., 1982. Microfossils from the Late Precambrian Draken Conglomerate, Ny Friesland, Svalbard. *J. Paleontol.* 56, 755–790.

Knoll, A.H., Simonson, B., 1981. Early Proterozoic Microfossils and Penecontemporaneous Quartz Cementation in the Sokoman Iron Formation, Canada. *Science* 211, 478–480. <https://doi.org/10.1126/science.211.4481.478>

Knoll, A.H., Swett, K., Mark, J., 1991. Paleobiology of a Neoproterozoic Tidal Flat/Lagoonal Complex: The Draken Conglomerate Formation, Spitsbergen. *J. Paleontol.* 65, 531–570.

Ma, J.F., Yamaji, N., Mitani, N., Xu, X.-Y., Su, Y.-H., McGrath, S.P., Zhao, F.-J., 2008. Transporters of arsenite in rice and their role in arsenic accumulation in rice grain. *Proc. Natl. Acad. Sci.* 105, 9931–9935. <https://doi.org/10.1073/pnas.0802361105>

Maliva, R.G., Knoll, A.H., Siever, R., 1989. Secular Change in Chert Distribution: A Reflection of Evolving Biological Participation in the Silica Cycle. *PALAIOS* 4, 519–532. <https://doi.org/10.2307/3514743>

Maliva, R.G., Knoll, A.H., Simonson, B.M., 2005. Secular change in the Precambrian silica cycle: Insights from chert petrology. *Geol. Soc. Am. Bull.* 117, 835–845. <https://doi.org/10.1130/B25555.1>

Marin, F., Smith, M., Isa, Y., Muyzer, G., Westbroek, P., 1996. Skeletal matrices, mucin, and the origin of invertebrate calcification. *Proc. Natl. Acad. Sci. U. S. A.* 93, 1554–1559.

Marron, A.O., Ratcliffe, S., Wheeler, G.L., Goldstein, R.E., King, N., Not, F., de Vargas, C., Richter, D.J., 2016. The Evolution of Silicon Transport in Eukaryotes. *Mol. Biol. Evol.* 33, 3226–3248. <https://doi.org/10.1093/molbev/msw209>

Martin-Jézéquel, V., Hildebrand, M., Brzezinski, M.A., 2000. Silicon Metabolism in Diatoms: Implications for Growth. *J. Phycol.* 36, 821–840. <https://doi.org/10.1046/j.1529-8817.2000.00019.x>

Muir, M.D., 1976. Proterozoic microfossils from the Amelia Dolomite, McArthur Basin, Northern Territory. *Alcheringa Australas. J. Palaeontol.* 1, 143–158. <https://doi.org/10.1080/03115517608619066>

Nelson, D.M., Riedel, G.F., Millan-Nunez, R., Lara-Lara, J.R., 1984. Silicon uptake by algae with no known Si requirement. I. True cellular uptake and pH-induced precipitation by *Phaeodactylum tricornutum* (bacillariophyceae) and *Platymonas* sp. (prasinophyceae). *J. Phycol.* 20, 141–147. <https://doi.org/10.1111/j.0022-3646.1984.00141.x>

Nimer, N.A., Brownlee, C., Merrett, M.J., 1994. Carbon dioxide availability, intracellular pH and growth rate of the coccolithophore *Emiliania huxleyi*. *Mar. Ecol. Prog. Ser.* 109, 257–262.

Price, N.M., Harrison, G.I., Hering, J.G., Hudson, R.J., Nirel, P.M.V., Palenik, B., Morel, F.M.M., 1989. Preparation and Chemistry of the Artificial Algal Culture Medium Aquil. *Biol. Oceanogr.* 6, 443–461. <https://doi.org/10.1080/01965581.1988.10749544>

Quigg, A., Finkel, Z.V., Irwin, A.J., Rosenthal, Y., Ho, T.-Y., Reinfelder, J.R., Schofield, O., Morel, F.M.M., Falkowski, P.G., 2003. The evolutionary inheritance of elemental stoichiometry in marine phytoplankton. *Nature* 425, 291–294. <https://doi.org/10.1038/nature01953>

Rasmussen, B., Krapež, B., Muhling, J.R., 2015. Seafloor silicification and hardground development during deposition of 2.5 Ga banded iron formations. *Geology* 43, 235–238. <https://doi.org/10.1130/G36363.1>

- Riedman, L.A., Sadler, P.M., 2018. Global species richness record and biostratigraphic potential of early to middle Neoproterozoic eukaryote fossils. *Precambrian Res.*, Descent into the Cryogenian 319, 6–18. <https://doi.org/10.1016/j.precamres.2017.10.008>
- Rogerson, A., DeFreitas, A.S.W., McInnes, A.G., 1987. Cytoplasmic silicon in the centric diatom *Thalassiosira pseudonana* localized by electron spectroscopic imaging. *Can. J. Microbiol.* 33, 128–131. <https://doi.org/10.1139/m87-022>
- Schopf, J.W., 1968. Microflora of the Bitter Springs Formation, Late Precambrian, Central Australia. *J. Paleontol.* 42, 651–688.
- Sergeev, V.N., Knoll, A.H., Grotzinger, J.P., 1995. Paleobiology of the Mesoproterozoic Billyakh Group, Anabar Uplift, Northern Siberia. *J. Paleontol.* 69, 1–37. <https://doi.org/10.1017/S0022336000062375>
- Sergeev, V.N., Knoll, A.H., Petrov, P.Yu., 1997. Paleobiology of the Mesoproterozoic-Neoproterozoic transition: the Sukhaya Tunguska Formation, Turukhansk Uplift, Siberia. *Precambrian Res.* 85, 201–239. [https://doi.org/10.1016/S0301-9268\(97\)00035-1](https://doi.org/10.1016/S0301-9268(97)00035-1)
- Siever, R., 1992. The silica cycle in the Precambrian. *Geochim. Cosmochim. Acta* 56, 3265–3272. [https://doi.org/10.1016/0016-7037\(92\)90303-Z](https://doi.org/10.1016/0016-7037(92)90303-Z)
- Siever, R., 1962. Silica Solubility, 0°–200° C., and the Diagenesis of Siliceous Sediments. *J. Geol.* 70, 127–150. <https://doi.org/10.1086/626804>
- Siever, R., Woodford, N., 1973. Sorption of silica by clay minerals. *Geochim. Cosmochim. Acta* 37, 1851–1880. [https://doi.org/10.1016/0016-7037\(73\)90146-4](https://doi.org/10.1016/0016-7037(73)90146-4)
- Sims, P.A., Mann, D.G., Medlin, L.K., 2006. Evolution of the diatoms: insights from fossil, biological and molecular data. *Phycologia* 45, 361–402. <https://doi.org/10.2216/05-22.1>
- Sperling, E.A., Robinson, J.M., Pisani, D., Peterson, K.J., 2010. Where's the glass? Biomarkers, molecular clocks, and microRNAs suggest a 200-Myr missing Precambrian fossil record of siliceous sponge spicules. *Geobiology* 8, 24–36. <https://doi.org/10.1111/j.1472-4669.2009.00225.x>
- Stefurak, E.J.T., Lowe, D.R., Zentner, D., Fischer, W.W., 2015. Sedimentology and geochemistry of Archean silica granules. *Geol. Soc. Am. Bull.* 127, 1090–1107. <https://doi.org/10.1130/B31181.1>
- Stefurak, E.J.T., Lowe, D.R., Zentner, D., Fischer, W.W., 2014. Primary silica granules—A new mode of Paleoproterozoic sedimentation. *Geology* 42, 283–286. <https://doi.org/10.1130/G35187.1>
- Sullivan, C.W., 1979. Diatom mineralization of silicic acid. IV. Kinetics of soluble Si pool formation in exponentially growing and synchronized *Navicula pelliculosa*. *J. Phycol.*
- Sunda, W.G., Price, N.M., Morel, F.M., 2005. Trace metal ion buffers and their use in culture studies. *Algal Cult. Tech.* 4, 35–63.
- Thametrakoln, K., Hildebrand, M., 2008. Silicon Uptake in Diatoms Revisited: A Model for Saturable and Nonsaturable Uptake Kinetics and the Role of Silicon Transporters. *Plant Physiol.* 146, 1397–1407. <https://doi.org/10.1104/pp.107.107094>
- Tiller, K.G., Pickering, J.G., 1974. The Synthesis of Zinc Silicates at 20°C and Atmospheric Pressure. *Clays Clay Miner.* 22, 409–416. <https://doi.org/10.1346/CCMN.1974.0220507>

- Trower, E.J., Fischer, W.W., 2019. Precambrian Si isotope mass balance, weathering, and the significance of the authigenic clay silica sink. *Sediment. Geol.* 384, 1–11. <https://doi.org/10.1016/j.sedgeo.2019.02.008>
- Tutolo, B.M., Tosca, N.J., 2018. Experimental examination of the Mg-silicate-carbonate system at ambient temperature: Implications for alkaline chemical sedimentation and lacustrine carbonate formation. *Geochim. Cosmochim. Acta* 225, 80–101. <https://doi.org/10.1016/j.gca.2018.01.019>
- Wever, P.D., O'dogherty, L., Caridroit, M., Dumitrica, P., Guex, J., Nigrini, C., Caulet, J.-P., 2003. Diversity of radiolarian families through time. *Bull. Société Géologique Fr.* 174, 453–469. <https://doi.org/10.2113/174.5.453>
- Williams, R.J.P., Rickaby, R.E.M., 2012. *Evolution's Destiny: Co-evolving Chemistry of the Environment and Life*. Royal Society of Chemistry.
- Wu, B., Beitz, E., 2007. Aquaporins with selectivity for unconventional permeants. *Cell. Mol. Life Sci.* 64, 2413–2421. <https://doi.org/10.1007/s00018-007-7163-2>
- Yates, D.M., Joyce, K.J., Heaney, P.J., 1998. Complexation of copper with polymeric silica in aqueous solution. *Appl. Geochem.* 13, 235–241. [https://doi.org/10.1016/S0883-2927\(97\)00062-0](https://doi.org/10.1016/S0883-2927(97)00062-0)
- Zhang, Q., T. Snow, J., Holdship, P., Price, D., Watson, P., M. Rickaby, R.E., 2018. Direct measurement of multi-elements in high matrix samples with a flow injection ICP-MS: application to the extended *Emiliana huxleyi* Redfield ratio. *J. Anal. At. Spectrom.* 33, 1196–1208. <https://doi.org/10.1039/C8JA00031J>

741    **Acknowledgements**

742    Errin Johnson helped with SEM analysis, and Phil Holdship assisted with ICP-MS analysis.  
743    Thank you to Sophie Gill, Roxana Shafiee, Ellen Cliff, Mahdi El Bendif, Samuel Eggins, and  
744    Steven Wyatt for help and advice in the laboratory. This work was supported by ERC  
745    consolidator grant APPELS agreement number 681746 to R Rickaby and NERC grant  
746    NE/M013014/1 to N Tosca and R Rickaby.

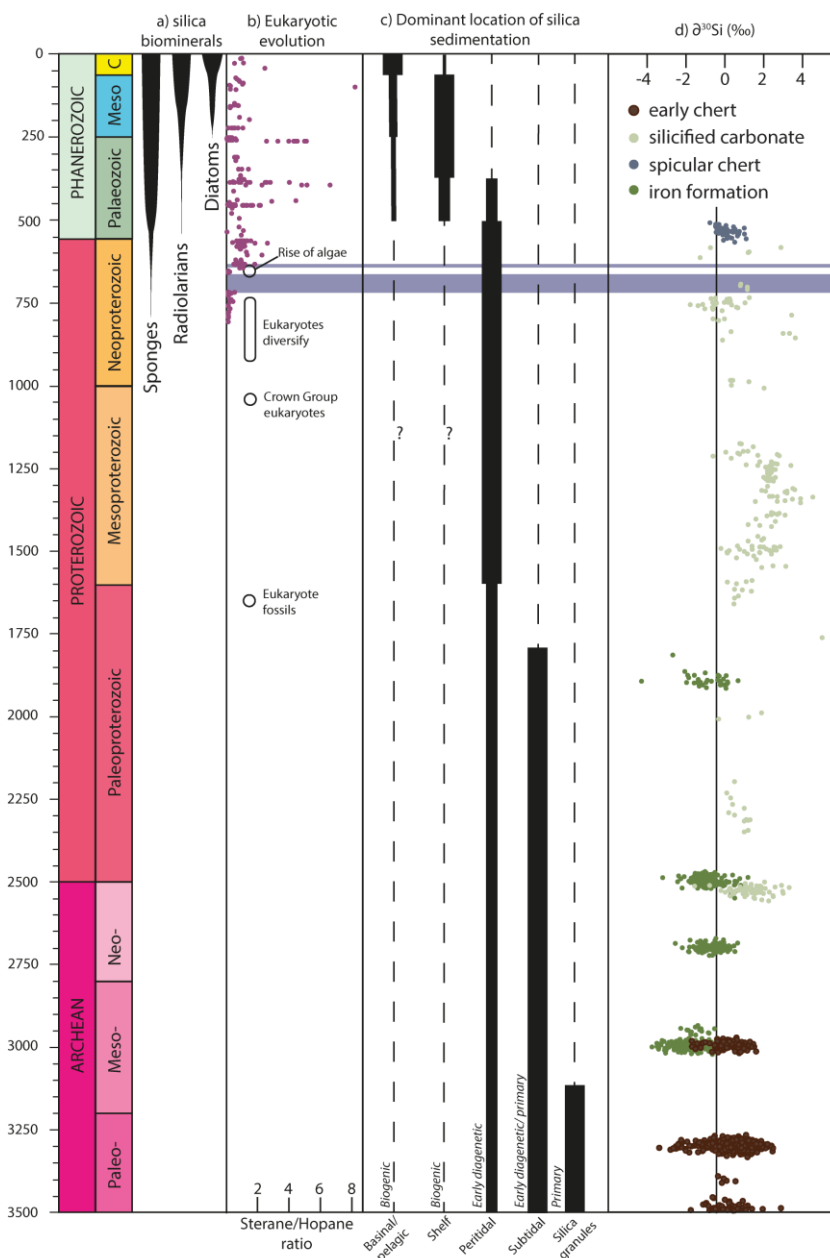


**Figure 1.** a) Summary of the evolution of siliceous organisms, where the width of the black lines indicates relative abundance through time. b) Sterane to hopane ratios from Brocks et al., (2017), indicating the ecological contribution of eukaryotes/prokaryotes to sedimentary organic carbon (purple circles) and key events in early eukaryotic evolution (open circles). c) Changes in the dominant location of silica sedimentation through time, where the width of the bar represents the relative importance of the sink (Maliva et al., 2005). d)  $\delta^{30}\text{Si}$  data from Trower and Fischer, (2019), from iron formation (dark green), spicular chert (blue),

silicified carbonate (light green), and early chert (dark brown) compared with bulk silicate Earth (black line).

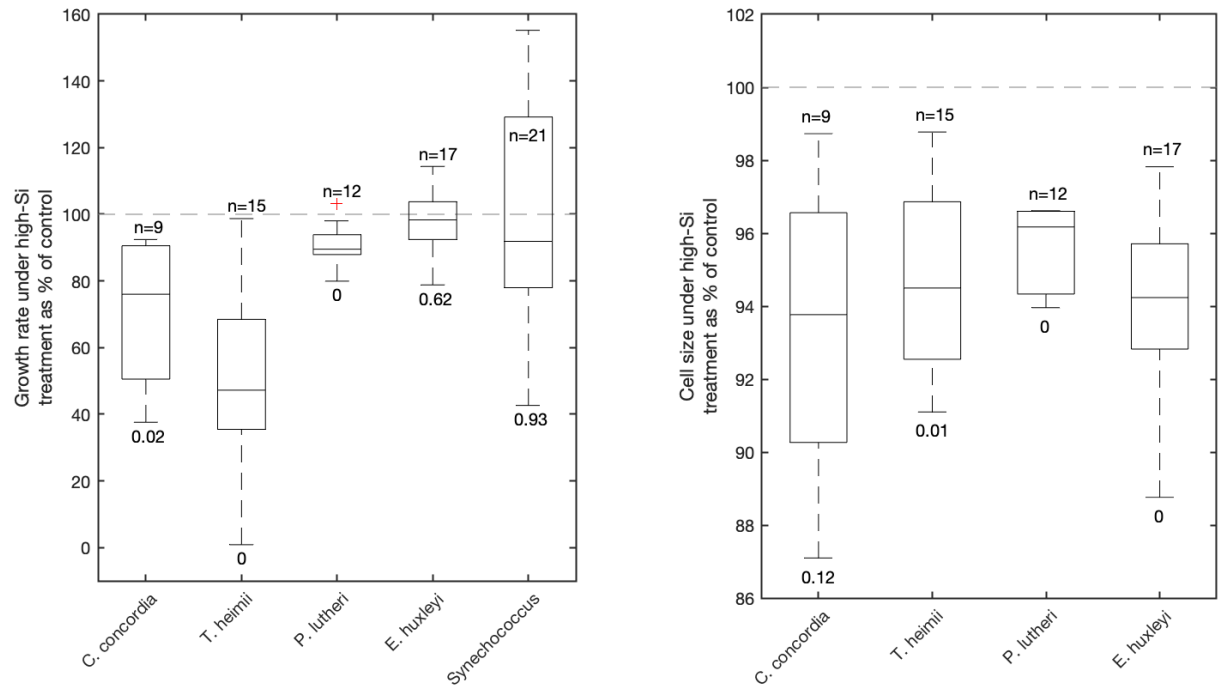


**Figure 2.** Box plots showing the maximum growth rates (left) and cell size at maximum

growth rates (right) for the high-Si treatment as a percentage of the control. The red crosses indicates an outlier. The result were calculated independently for ‘n’ independent replicate cultures. The values below the bars are P-values for one-way Anova tests, rounded to two decimal digits (i.e. values of 0 represent  $p < 0.01$ ). Values  $< 0.05$  indicate that the means of the two groups are significantly different. *C. concordia*, *T. heimii*, and *P. lutheri* show reduced growth rates, and *C. concordia*, *T. heimii* and *E. huxleyi* show reduced cell size.



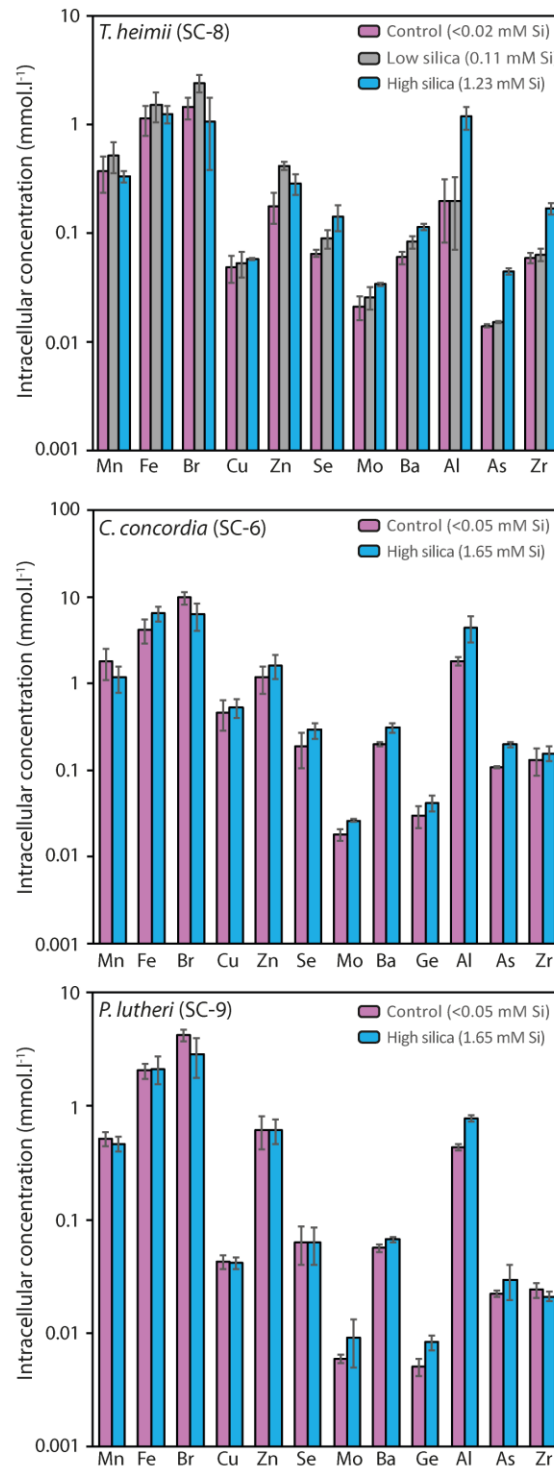


**Figure 3.** Intracellular metal concentration for cells grown in control, low silica and high silica media. Each bar represents the average of triplicate cultures grown under identical conditions, and the error bar represents one standard deviation.

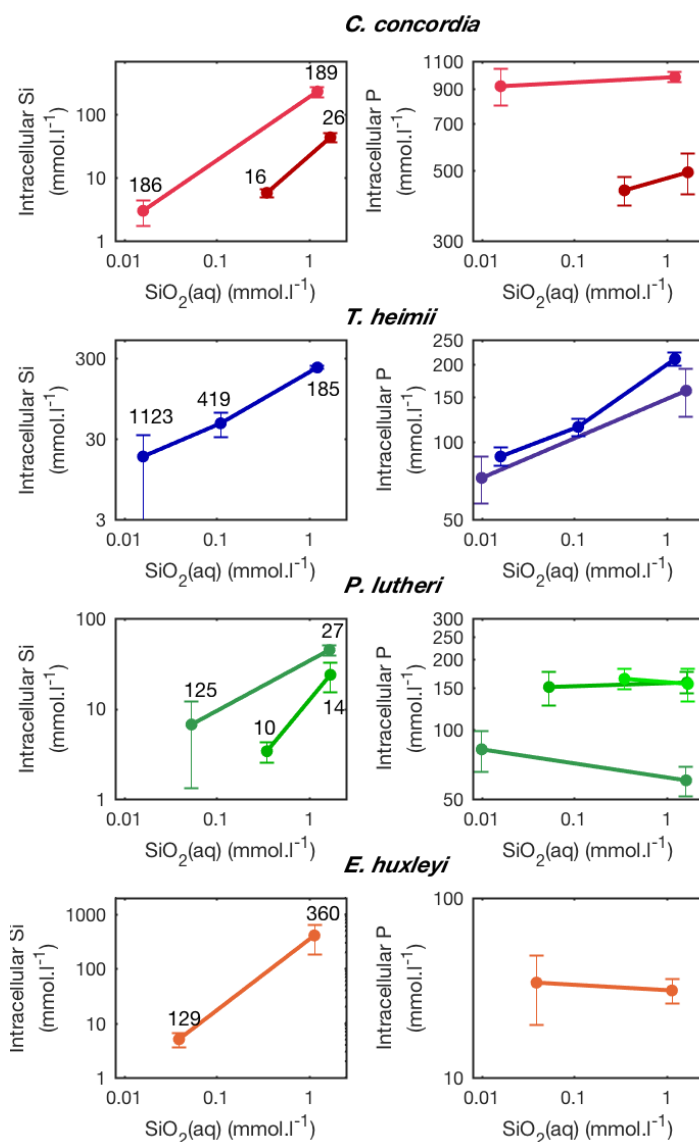


**Figure 4.** Intracellular Si and P concentrations for each species compared with the Si

concentration in the culture media. The intracellular concentrations were calculated from

total digestions, and the cell counts and cell diameters when cells were harvested. Each data

point represents the average of triplicate cultures grown under identical conditions, and the

error bar represents one standard deviation. Each coloured line represents cells harvested

from independent sub-cultures. The ratio of intracellular Si to Si in the media (enrichment

factor) is listed next to each data point. Note that the error associated with the calculated

enrichment factor is larger when Si concentrations are lower.

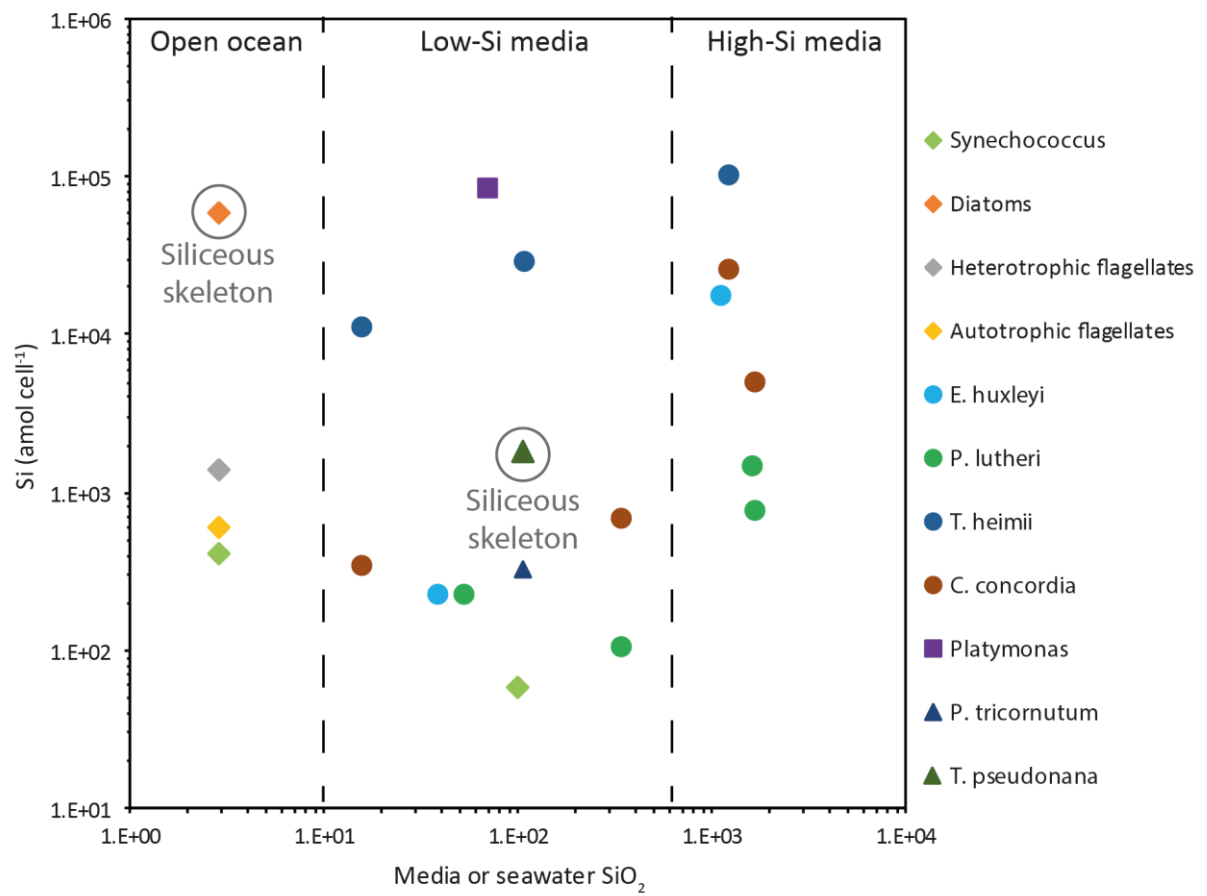


**Figure 5:** Intracellular silica concentration, in amol. cell<sup>-1</sup>, for a range of algal species with no known silica requirement. Data are from Baines et al., (2012) (diamonds); Fuhrman et al., (1978) (square); D'Elia et al., (1979) (triangles); and this study (circles). Cells from the open ocean come from equatorial upwelling regions of the Pacific Ocean.

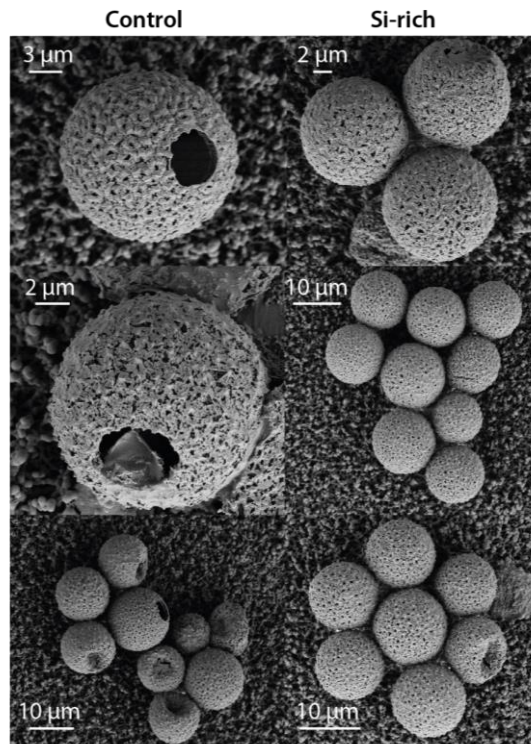


**Figure 6.** SEM images of *T. heimii* grown under control conditions (left) and in high-silica media (right). Note the visible excystment opening under control conditions.